Journal of Electroanalytical Chemistry 902 (2021) 115812

Contents lists available at ScienceDirect

Journal of Electroanalytical Chemistry

journal homepage: www.elsevier.com/locate/jelechem

Vanadium doped nickel cobalt phosphide as an efficient and stable electrode catalyst for hydrogen evolution reaction

Xiao Li, Yuanjian Liu, Yudong Wu, Shanshan Li, Yinchen Dai, Jibiao Guan, Ming Zhang *

National Engineering Lab for Textile Fiber Materials and Processing Technology, Zhejiang Sci-Tech University, Hangzhou 310018, PR China

ARTICLE INFO

Keywords:
Doping
Electrocatalyst
Bimetallic phosphide

ABSTRACT

Though transition metal phosphides (TMPs) have been applied as an efficient and cost-effective catalyst for hydrogen evolution reaction (HER), their large-scale application is still restrained by their lack of activity and durability. In this work, a novel vanadium doped nickel cobalt phosphide catalyst supported on carbon cloth (V-NiCoP/CC) is fabricated by a facile hydrothermal and phosphate method. Remarkably, V-NiCoP/CC only need the overpotential of 52 mV to drive 10 mA cm^{-2} in 1 M KOH solution, which is superior to many state-of-art transition monometallic phosphides electrocatalysts. Meanwhile, V-NiCoP/CC exhibits a low tafel slope of 51.2 mV dec^{-1} and superior stability in 2000 CV cycles and 40 h of long-term stability test. Furthermore, this work verifies that doping heteroatom provides new opportunities to enhance the HER performance of transition bimetallic phosphides with effect on their morphology and electrochemical properties.

1. Introduction

With the huge consumption of traditional fossil fuel and unrecoverable pollution, the development and utilization of more new energy sources have attracted worldwide attention. Hydrogen, as a kind of efficient, clean and pollution-free new energy, is considered as the most likely alternative to conventional fossil fuels, and has great ability to solve the problem of energy crisis [1–3]. Among the existing hydrogen production technologies, electrocatalytic water splitting, which consists of cathode hydrogen evolution reaction (HER) and anode oxygen evolution reaction (OER), is a clean and sustainable effective strategy [4–6]. Although electrolysis of water for hydrogen production requires a large overpotential to overcome the slow kinetic and takes a small share in industrial production, it has obvious advantages due to its relatively simple equipment, only consumption of water and electricity, and no CO_2 generation [7–9]. Hence, it is extremely urgent to exploit the efficient and stable electrocatalysts to improve the performance of HER for mass production [10]. Although Pt based catalysts are considered as the most efficient catalysts toward HER, the scarcity and high price of Pt limit its large-scale application [11–13]. Transition metals (TMs), as an important member of these nonprecious metal catalysts, are regarded as promising substitutes for noble metals. Therefore, non-noble metal electrocatalysts as Pt-based catalysts substitutes have been widely studied [14,15]. In recent years, massive efforts have been committed to designing cost-efficient and earth abundant noble-metal-based electrocatalysts alternatives to improve the efficiency of electrocatalysis, such as sulfides [16], selenides [17], phosphides [18] and carbides [19].

Among of these, transition mental phosphides (TMPs), for instance, Ni_2P [20], CoP [21], CoP_2 [22], and MoP [23] have recently been researched in the search for alternative transition metal compounds that can achieve the performance of Pt-based catalysts owing to their low cost and high intrinsic activity [24,25]. Bimetallic phosphide exhibit better catalytic performance than monometallic phosphides due to the alteration of electronic structure [26–28]. Similarly, heteroatom-doping can further improve performance by changing the state of charge [29–31]. Vanadium, as the earth-abundant and efficient mental, which can tune the electronic properties [32] and enhance the conductivity of the materials [33], has proved to be an excellent dopant in electrochemical catalysts. For example, Wang's team has successfully incorporated vanadium into $Co(OH)_2$ and formed a CoV-layered double-layer hydroxide (LDH), which yielded excellent performance in electrolysis of water for hydrogen production [34]. The excellent catalytic activity of CoV-LDH is attributed to its enhancement of catalyst conductivity, acceleration of electron transfers and enrichment of electrochemical active centers, which indicates that vanadium will be a good foreign dopant. Chen's team successfully prepared Ru-doped 3D flower-like bimetallic phosphide catalyst for overall water splitting, demonstrating excellent performance [35]. The design and preparation of bimetallic phosphide can coordinate different metal ions and

* Corresponding author.
E-mail address: zhangming@zstu.edu.cn (M. Zhang).

https://doi.org/10.1016/j.jelechem.2021.115812
Received 30 June 2021; Received in revised form 26 September 2021; Accepted 19 October 2021
Available online 28 October 2021

change the electronic structure of the catalysts, so as to improve the catalytic performance, indicating that NiCoP bimetallic phosphide has better electrocatalytic activity than its relevant single metal phosphide.

Based on the above discussion, we herein bring forward a scheme that vanadium doped in the nanoneedles of nickel and cobalt phosphide compounds synthesized through a hydrothermal-phosphorization method. The hydrothermal phosphating method can be used to synthesize the electrocatalyst with high activity and good stability on a large scale. The effect of V doping was analyzed by morphology characterization and electrochemical performance test, and it was confirmed that the introduction of V indeed increased the exposure of the active surface and improved the electrical conductivity. In addition, the effects of different molar amount of V additive (0, 5%, 10%, 15%) on its morphology and properties were also studied. When the addition amount of V is 10%, V-NiCoP/CC only need the overpotential of 52 mV to obtain the current of 10 $mA{\cdot}cm^{-2}$ in 1 M KOH solution. What's more, V-NiCoP/CC demonstrates excellent stability, essentially the same after 2000 CV cycles, and the current density remains basically unchanged for as long as 40 h. Therefore, this kind of V-NiCoP/CC electrode material has great potential as a high-performance hydrogen production device.

2. Experiments

2.1. Materials

All chemicals include Nickel nitrate hexahydrate ($Ni(NO_3)_2{\cdot}6H_2O$, Shanghai McLean Biochemical Co., Ltd), cobalt nitrate hexahydrate ($CO(NO_3)_2{\cdot}6H_2O$, Shanghai McLean Biochemical Co., Ltd), vanadium Chloride (III) (VCl_3, Shanghai San'an Chemical Technology Co., Ltd), Urea (CH_4N_2O, Shanghai Aladdin Biochemical Technology Co., Ltd) and sodium hypophosphite (NaH_2PO_2, Shanghai Aladdin Biochemical Technology Co., Ltd) and carbon cloth (CC, WOS1009, China Power Technology Co., Ltd). Except for the carbon cloth, all materials were used without further treatment.

3. Preparation of V-NiCoP/CC

The substrate CC ($1 \times 4\ cm^2$) was treated with concentrated nitric acid at 90℃ for 2 h, then cleaned sequentially in ethanol and deionized water for 20 min. The preparation of V-NiCoP/CC nanoneedle arrays on the CC is a simple hydrothermal process and phosphating treatment. In a typical synthesis, 1 mmol of ($Ni(NO_3)_2{\cdot}6H_2O$), 1 mmol of ($Co(NO_3)_2{\cdot}6H_2O$), 0.2 mmol of VCl_3, and 10 mmol $CO(NH_2)_2$ were dissolved in 30 mL of deionized water under vigorous stirring. Afterwards, the treated CC was immersed into the solution and transferred into Teflon-lined stainless steel autoclave, and then reacted at 120℃ for 6 h in an electric oven. After cooling to room temperature, the CC with the active materials was taken out and washed by deionized water, and then dried at 60℃ for a whole night. To obtain V-NiCoP/CC, the precursor and 0.5 g NaH_2PO_2 were put into a tube furnace, and then annealed at 350℃ for 2 h with a heating rate of 5℃ min^{-1} in an Ar atmosphere. The V_x-NiCoP/CC (x represents different vanadium doping levels, x = 0, 0.05, 0.15) were also prepared with the same method. What's more, the $V_{0.10}$-Ni_yCo_{2-y}/CC (y represents the molar ration of Ni and Co in the as-prepared materials, y = 0, 0.5, 1.0, 1.5, 2.0) were also prepared.

4. Material characterization

The X-ray diffraction (XRD, Bruker AXS GmbH, Germany) test was conducted at an angle range of 10-90° with a working voltage of 40 kV. The morphology and chemical element composition of the catalyst were characterized by scanning electron microscopy (SEM, JSM-6700, JEOL, Japan) and energy dispersive X-ray spectrometry (EDX), respectively. The crystal structures were observed by transmission electron microscopy (TEM, JSM-2100, JEOL, Japan). X-ray photoelectron spectroscopy (XPS) was conducted on a Kratos Axis Ultra DLD with an Al (mono) K source (1486.6 eV).

5. Electrochemical measurements

All the electrochemical tests were performed in a three electron electrochemical cell using the CHI 660D electrochemical workstation (CH Instruments, Inc., Shanghai). The prepared samples, Hg/HgCl electrode, and a graphite rod were used as the working electrode, reference electrode, and counter electrode, respectively. Linear sweep voltammograms (LSVs) were tested at 1 mV s^{-1} and the saturated calomel electrode (SCE) was calibrated with respect to reversible hydrogen electrode (RHE) ($E_{RHE} = E_{SCE} + 0.244 + 0.0592 \times pH$). The tafel slope was acquired by fitting the polarization with the Tafel equation ($\eta = b \log|j| + a$, where η is overpotential, j is current density and b is tafel slope). Cyclic voltammograms (CV) were recorded to obtain electrochemical surface areas (ECSA) at different scan rates from 10 mV s^{-1} to 100 mV s^{-1}. The roughness factor (Rf) was calculated by taking the estimated ECSA and dividing by the geometric area of the electrode. Electrochemical impedance spectra (EIS) were measured over the frequency range from 100 kHz to 0.01 Hz.

6. Results and discussion

The preparation process of the V-NiCoP/CC is described in Fig. 1. The vanadium doped nickel cobalt precursor was grown on carbon cloth by one-step hydrothermal, and then calcined at 350 ℃ with the $NaHPO_2$ as P source. As shown in scanning electron microscopy (SEM) of Fig. S1a-b, nickel cobalt phosphide nanoneedles are uniformly and densely grown on carbon cloth. The acupuncture-shaped structure provides a larger specific surface area for water contacting and hydrogen atom absorption, theoretically providing more active sites for HER. As shown in Fig. 2 a-b, the images maintain the same nanoneedles structure with V dopant, indicating that vanadium didn't cause a fundamental change in morphology. Meanwhile, compare with the precursor of Ni and Co compounds (Fig. S2a-b and Fig. S3a-b), phosphating also didn't change the morphology. However, the size of the V-NiCoP is slightly larger than that of pure NiCoP, which indicates that the introduce of V effectively regulate the morphology of NiCoP. Moreover, different V doping amounts (Fig. S4a-b) also showed a denser morphology and the ultra-fine nanoneedles of small size can release more active sites for HER process [36–38]. For further analyze the structure of V-NiCoP/CC, high-resolution transmission electron microscope (HRTEM) was used to explore the nanostructure and elementary composition. As shown in Fig. 2c-d, the interlayer spacing of 0.251, 0.193 and 0.227 nm are attributed to the (201), (200) and (111) planes of NiCoP crystals, respectively. In order to further investigate the distribution of elements on the V-NiCoP/CC, Fig. 2e-i display the corresponding energy dispersive X-ray (EDX) elemental mapping images of Ni, Co, V, P for the V-NiCoP/CC, in which that Ni, Co, V, P is completely distributed on V-NiCoP/CC and further prove that V is successfully introduced in NiCoP/CC. In addition, as EDX spectrum of V-NiCoP/CC shown in Fig. S5, it displays the relative content of the elements. And the weight ratio of Ni: Co: V: P elements is about 0.24: 0.26: 0.04: 0.46 in Table S1, where the ratio of Ni and Co is also close to the feed ratio. In addition, other vanadium doping amounts are also listed in Table S1.

X-ray diffraction (XRD) was further applied to explore the crystal phase and composition after the addition of vanadium. The diffraction peaks at 41.0°, 44.9° and 47.6° correspond to the (111), (201) and (210) planes of NiCoP crystals, respectively (Fig. 3a). The peaks basically correspond to JCPDS no.71–2336, indicating that no new phase

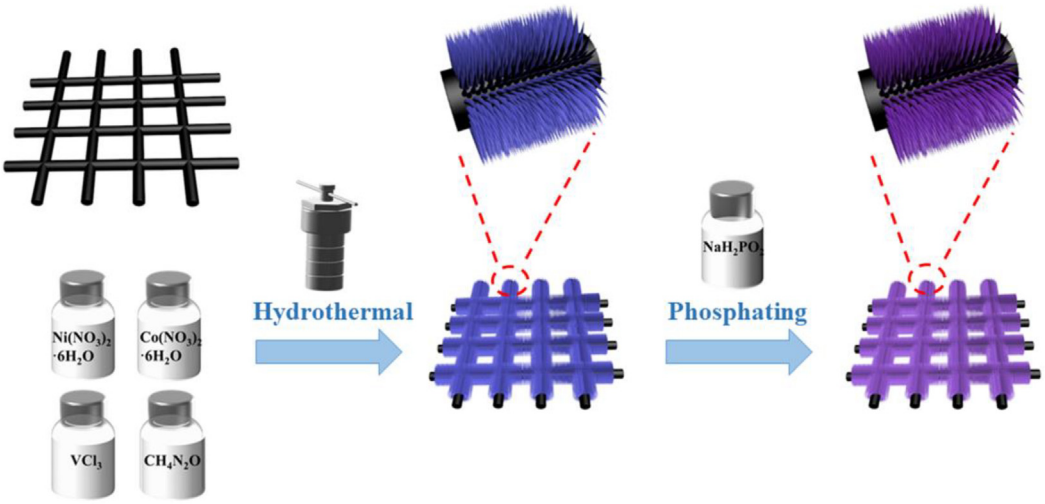

Fig. 1. Schematic illustration of the process of V-NiCoP/CC.

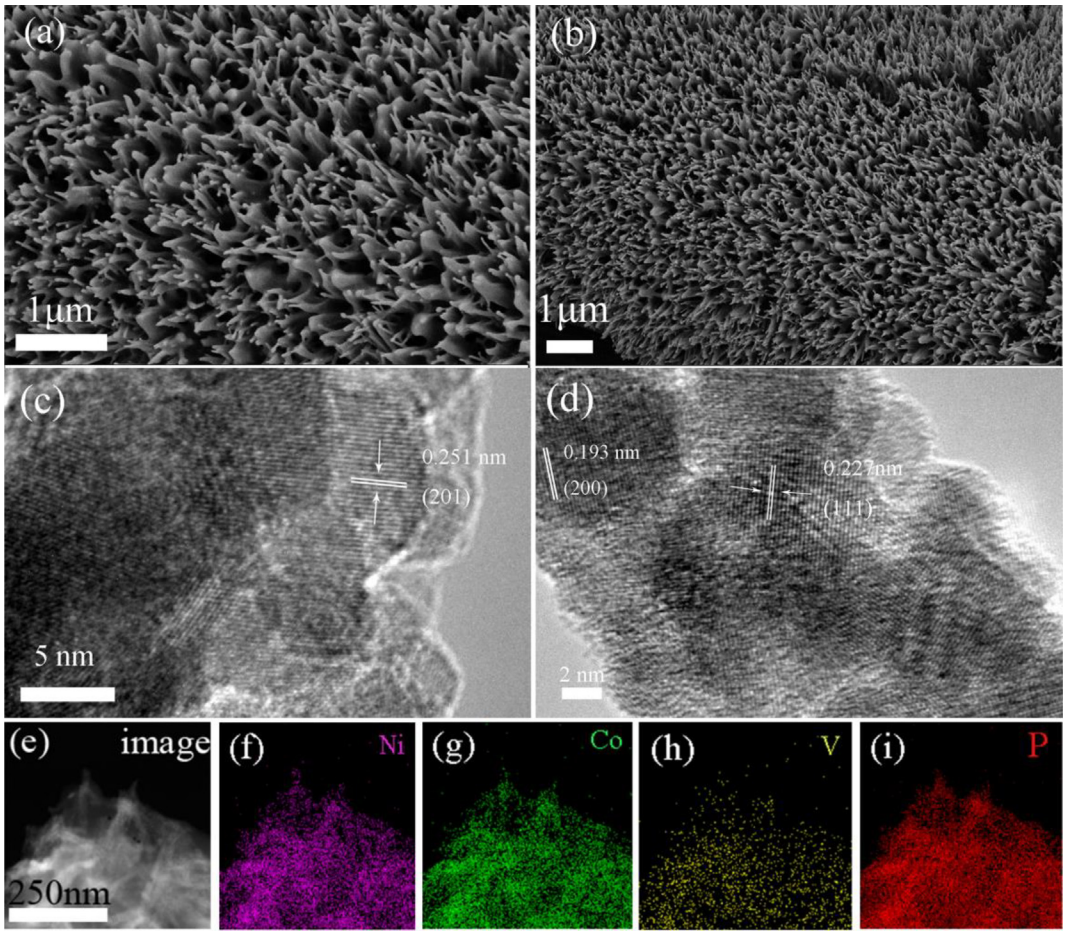

Fig.2. SEM images of V-NiCoP/CC at (a) 20 k magnifications. (b) 10 k magnifications. (c and d) HRTEM images of V-NiCoP/CC. (e-h) EDX elemental mapping of V-NiCoP/CC.

produced after the introduction of vanadium. In addition, Fig. S6 shows the XRD results of different vanadium doping levels (0, 5%, 10% and 15%). This confirms the successful incorporation of vanadium and absence of vanadium compounds. Based on XRD results, the elemental composition of NiCoP/CC and V-NiCoP/CC were studied with X-ray photoelectron spectroscopy (XPS). Fig. 3b shows the survey XPS diffraction pattern of NiCoP/CC and V-NiCoP/CC, and they have the same pattern, except for a weak peak attributed to the V 2p, which indicates the presence of vanadium. In addition, C and O in the peak spectrum were caused by material pollution and surface oxidation [39]. Taking pure NiCoP/CC as a contrast, from the high resolution spectrum of Ni 2p (Fig. 3c), the peaks at 856.8 eV and 853.2 eV corre-

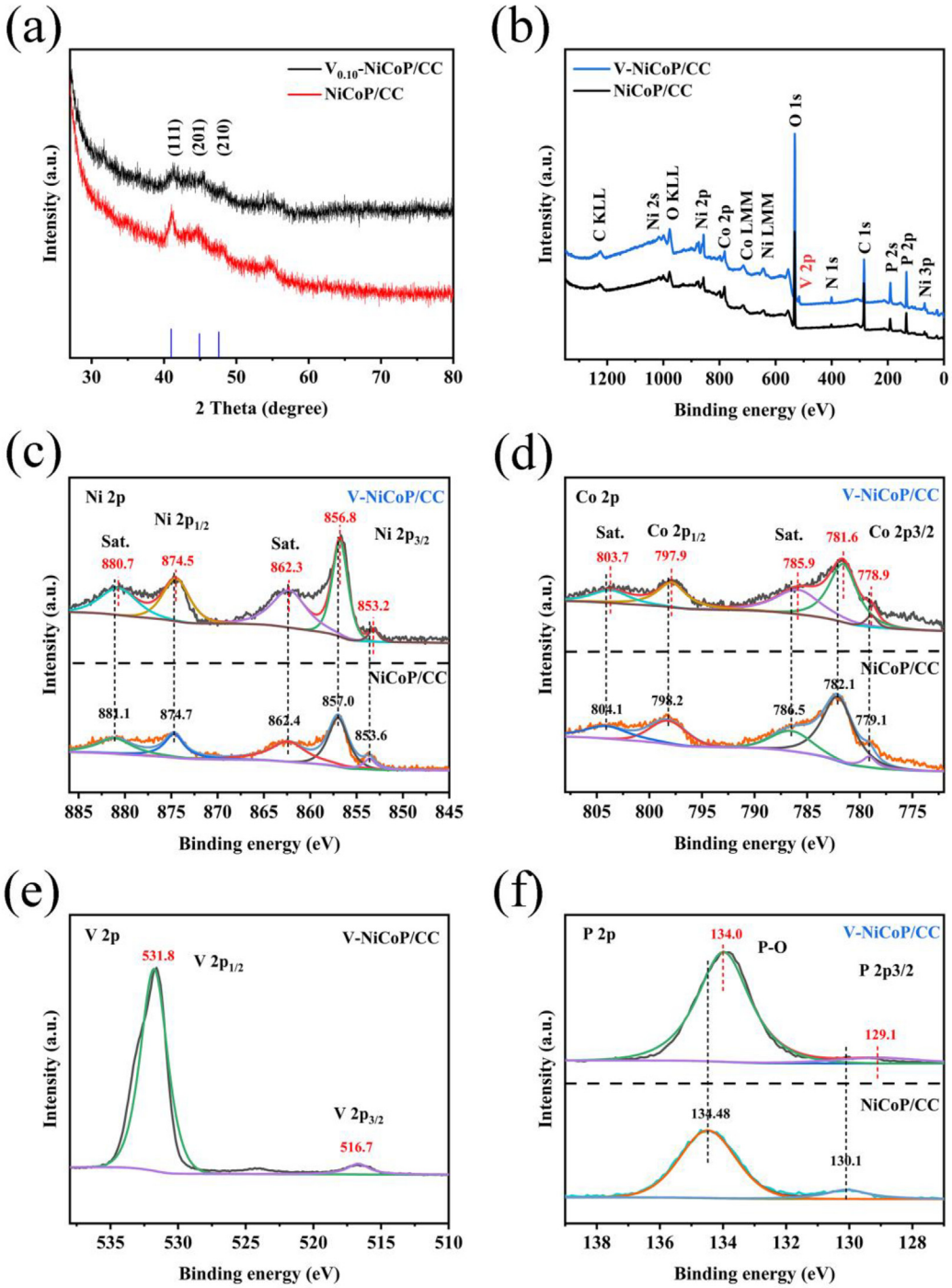

Fig.3. (a) XRD patterns of NiCoP/CC and V-NiCoP/CC. XPS spectra of V-NiCoP/CC in the (b) survey, (c) Ni 2p, (d) Co 2p, (e) V 2p and (f) P 2p.

spond to Ni $2p_{3/2}$ in V-NiCoP/CC [36,40], and their electronic intensity is slightly lower than that of pure NiCoP/CC. Similar to the Ni element, as shown in Fig. 3d, the Co $2p_{3/2}$ spectrum of V-NiCoP/CC can be divided into Co^{2+} (781.6 eV) and Co^{3+} (778.9 eV) with a satellite peak (785.9 eV) [41,42]. The binding energies (BEs) at 797.9 eV and 803.7 eV are assigned to Co $2p_{1/2}$ and satellite peaks, respectively. Overall, the BEs of Ni 2p and Co 2p in V-NiCoP/CC are slightly lower than pure NiCoP/CC, implying Ni and Co have partial negative charges. This result indicates that the electronic density is increased after V dopant and therefore improve the HER performance of electrocatalysis [43]. In the V 2p region, as shown in Fig. 3e, it is evident that belongs to V $2p_{3/2}$ at the peak of 516.7 eV and V $2p_{1/2}$ at 531.8 eV [37,44], which results from surface oxidation owing to exposure in air [45] and the formation of V-P bond [46]. In addition, the binding bond between P and metal (Fig. 3f) is observed in the 129.1 eV peak in the P 2p region [47], and 134.0 eV of the peak comes from the phosphorus oxide formed on the surface of the material or surface oxidation [48,49]. Meanwhile, compared with pure NiCoP, the peaks for Ni, Co and P in V-NiCoP shift to lower BEs, indicating that the addition of vanadium increased the electron density of NiCoP and there is a strong electron interaction between Ni, Co and V in the V-NiCoP system. Through the above discussion, it can be seen that V element is successfully doped into NiCoP/CC without a mixture of NiCoP and V-based phosphides.

Finally, the HER activity of different catalysts was tested by a typical three-electrode system in 1 M KOH with Hg/HgCl electrode as reference electrode, a graphite rod as the counter electrode and the sample as the working electrode. The results show that the polarization curves of $V_{0.01}$-$Ni_yCo_{2-y}P$/CC (y = 0, 0.5, 1, 1.5, 2) in Fig. 4a. Different ratios of Ni and Co show great difference, where $V_{0.01}$-NiCoP/CC exhibits the best performance. It only requires an overpotential of 52 mV to drive a current density of 10 mA cm^{-2}, which is superior to $V_{0.01}$-Ni_2P/CC (88 mV), $V_{0.01}$-$Ni_{1.5}Co_{0.5}P$/CC (71 mV), $V_{0.01}$-$Ni_{0.5}Co_{1.5}P$/CC (75 mV) and $V_{0.01}$-Co_2P/CC (84 mV). In addition, the tafel slope is also an important index to measure the kinetics of HER. $V_{0.01}$-NiCoP/CC shows a smaller tafel slope of 51.2 mV dec^{-1} than $V_{0.01}$-Ni_2P/CC (86.0 mV dec^{-1}), $V_{0.01}$-$Ni_{1.5}Co_{0.5}P$/CC (67 mV dec^{-1}), $V_{0.01}$-$Ni_{0.5}Co_{1.5}P$/CC (61 mv dec^{-1}) and $V_{0.01}$-Co_2P/CC (61.9 mv dec^{-1}). This further confirms that the ratio of Ni and Co can affect the process of HER and the increased kinetic activity may be attributable to the small charge transfer resistance. In order to further explain whether the increase in activity is related to the charge transfer resistance (R_{ct}, curvature of capacitor semicircle), an electrochemical impedance spectroscopy (EIS) test was carried out. As shown in Fig. 4c, V0.01-NiCoP/CC shows a smaller resistance value, compared with other ratios of Ni and Co. Besides, considering that the HER process may be affected by different active surface areas, we tested the cyclic voltammetry (CV) under different sweep rates to obtain the value of the double-layer capacitance (C_{dl}) to calculate the electrochemical active surface area (ECSA). According to the calculation (ECSA = C_{dl}*-S/C_s, C_{dl} is the double-layer capacitance, S is the geometric area of the electrode and C_s is the capacitance of the sample), ECSA and C_{dl} are positively correlated, that is, a larger C_{dl} means a larger ECSA [50–52]. For our estimates of ECSA, we use general specific capacitances of C_s = 0.040 mF cm^{-2} in 1 M KOH [53]. As shown in Fig. S7, 10 mV s^{-1} to 100 mV s^{-1} of CV curves were tested for catalysts with different ratios of Ni and Co. The calculated results in Fig. 4d show that $V_{0.01}$-NiCoP/CC display a C_{dl} value of 64.2 mF cm^{-2}, which is much larger than that of $V_{0.01}$-Ni_2P/CC (35.5 mF cm^{-2}), $V_{0.01}$-$Ni_{1.5}Co_{0.5}P$/CC (52.7 mF cm^{-2}), $V_{0.01}$-$Ni_{0.5}Co_{1.5}P$/CC (56.8 mF cm^{-2}) and $V_{0.01}$-Co_2P/CC (42.1 mF cm^{-2}). From the above discussion, $V_{0.01}$-NiCoP/CC shows better HER property compared with other Ni and Co ratios. Therefore, in the optimal ratio of Ni and Co, we focus on seeking and analyzing an optimal result by changing the doping amount of vanadium.

Different amounts of vanadium (0, 5%, 10% and 15%) doped in NiCoP/CC were tested in Fig. 5a, in which $V_{0.01}$-NiCoP/CC showed the best HER performance. Therefore, unless otherwise noted, the following analysis is $V_{0.01}$-NiCoP/CC. As expected, Pt/C possesses the highest HER electrocatalytic performance, especially at high current densities. Compared to other different doping levels, when the current density of 10 mA cm^{-2} is reached, V-NiCoP/CC only needs the ultralow overpotential of 52 mV, even the same as Pt/C catalyst. It is a significant improvement over pure NiCoP/CC (80 mV), $V_{0.05}$-NiCoP/CC (66 mV), and $V_{0.15}$-NiCoP/CC (64 mV). In addition, the comparison of HER performance between V-NiCoP/CC and other catalysts were shown in the followed Table S2. In addition to these, V-NiCoP/CC shows a smaller Tafel slope of 51.2 mV dec^{-1} than pure NiCoP/CC (71 mV dec^{-1}), $V_{0.05}$-NiCoP/CC (64.8 mV dec^{-1}), and $V_{0.15}$-NiCoP/CC (59.74 mv dec^{-1}). Additionally, tafel slope of Pt/C is 35.9 mV dec^{-1}. This also proves that V doping improves HER dynamics and accelerates electron transfer.

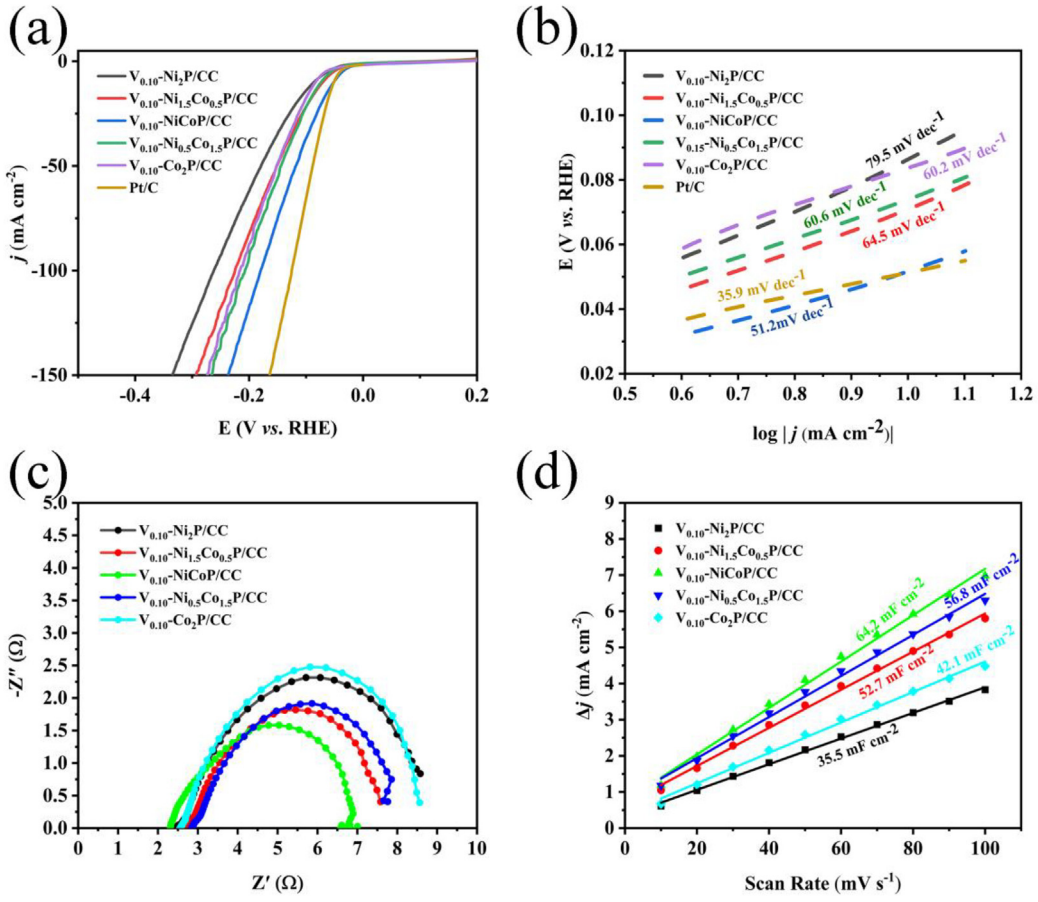

Fig. 4. The electrocatalytic measures of V0.01-NiyCo2-yP/CC (y = 0, 0.5, 1, 1.5 ,2) in 1 M KOH. (a-d) LSV polarization curves, Tafel plots, Nyquist plots and the Cdl measurements.

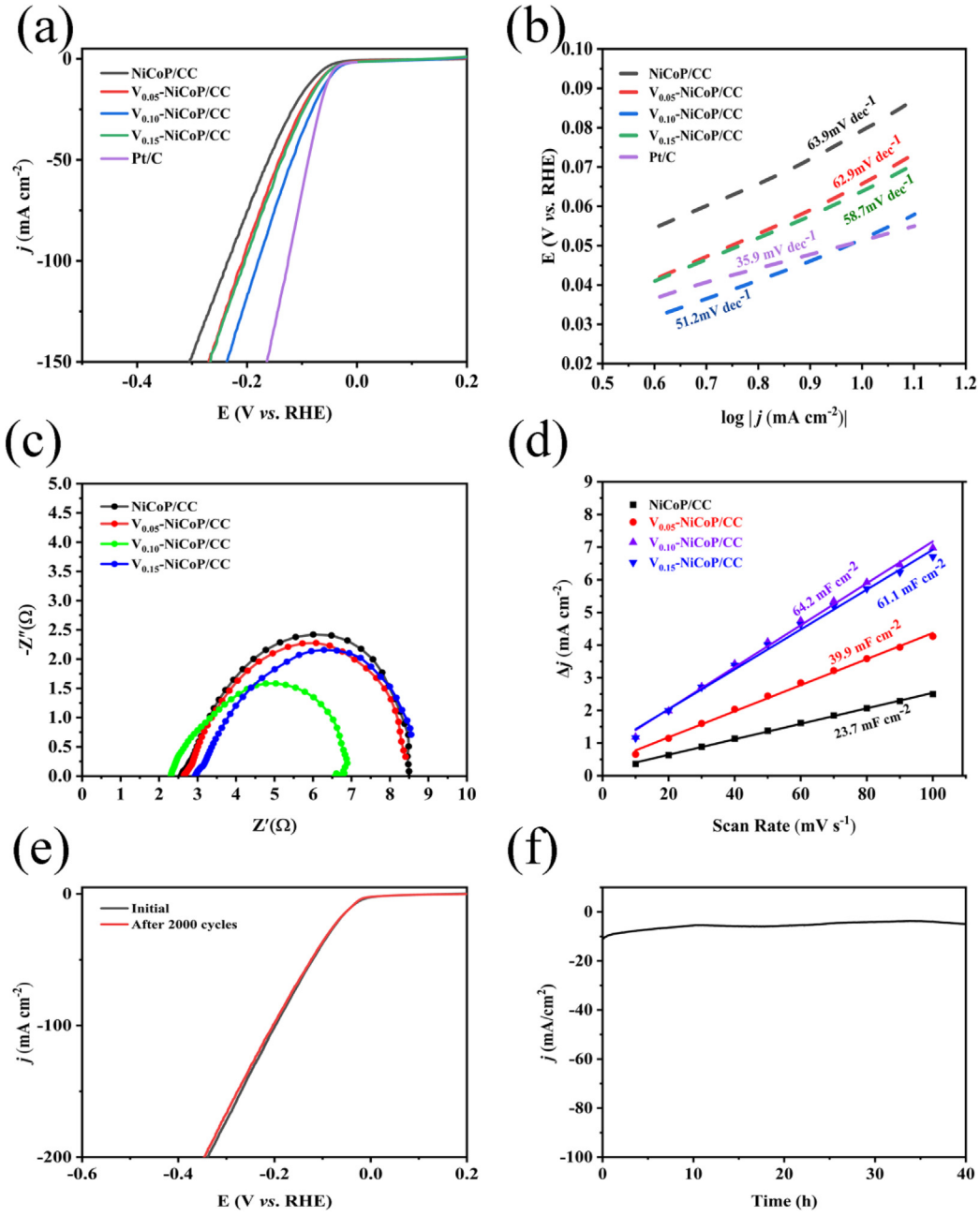

Fig.5. The electrocatalytic measures of V_x-NiCoP/CC (x = 0, 0.05, 0.10, 0.15) in 1 M KOH. (a-d) LSV polarization curves, Tafel plots, Nyquist plots and the C_{dl} measurements of V_x-NiCoP/CC and Pt/C. (e) Polarization curves of V-NiCoP/CC at the first cycle and after 2000 cycles. (f) The chronopotentiometric curve with a constant current density of 10 mA cm^{-2} for 40 h in 1 M KOH.

In order to further reveal the improved HER performance of V-NiCoP/CC, EIS analysis was performed on different doping amounts. From the Nyquist curves shown in Fig. 5c, with the same experimental conditions, it can be seen that all electrode resistances are small and similar. The low resistance values reflect fast reaction rates. Among of these, V-NiCoP/CC shows a smaller resistance value, indicating that the electron transport rate is improved and the reaction kinetics of HER is much faster after V doping. Besides, the exposure of more electrochemically active sites may be another reason to enhance the performance of HER. As shown in Fig. S8, 10 mV s^{-1} to 100 mV s^{-1} of CV curves were tested for catalysts with different doping amounts. The calculated results show that V-NiCoP/CC showed a C_{dl} value of 64.2 mF cm^{-2}, which is much larger than that of pure NiCoP/CC (23.7mF cm^{-2}). It is also better than $V_{0.05}$-NiCoP/CC (39.9 mF cm^{-2}) and $V_{0.15}$-NiCoP/CC (61.1 mF cm^{-2}), which demonstrates that V-doped catalyst exposes more active sites. Furthermore, the roughness factor (Rf) was shown in Table S3, which also indicates a greater promotion for HER with V dopant.

Stability is also an important index for hydrogen evolution, especially in practical application. Therefore, the sample was first tested by LSV with a sweep rate of 1 mV s^{-1}, and the overpotential of the current density at 10 mA cm^{-2} could be seen through the polarization curve. As shown in Fig. 5e, after 2000 CV cycles, the polarization curve of V-NiCoP/CC is almost the same as the initial one. Then, a long-term stability test was carried out by chronopotentiometry. Impressively, the current density remains basically unchanged for as long as 40 h, which indicates that the V-NiCoP/CC electrode material has a good stability. What's more, after I-T test, SEM images of sample is basically

similar to the original one (Fig. S9). Comparison of spectra of material before and after 40 h-long HER indirectly reveals that Ni, Co and V have partial negative charges with the decrease of BEs (Fig. S10a-c). The increase of binding energy of P indirectly indicates that partial oxidation occurs in HER process (Fig. S10d) and the corresponding peak at 129.9 eV can be attributed to the phosphide signal [54]. Moreover, TEM images of V-NiCoP/CC were recovered after 40 h-long electrocatalytic HER in Fig. S11. The lattice fringe spacing was essentially unchanged, indicating that the oxidation was not obvious during the HER. In addition, Fig. S12 displays the corresponding energy dispersive X-ray (EDX) elemental mapping images of Ni, Co, V, P for the V-NiCoP/CC after I-T test, in which the weight ratio of Ni: Co: V: P elements is about 0.39: 0.36: 0.02: 0.23 in Table S1, where the ratio of Ni and Co is basically unchanged. In brief, through 2000 CV cycles and 40 h of long-term stability test, it is proved that V-NiCoP/CC retains the original crystal morphology and have good material stability. In addition, the V-NiCoP/CC electrode shows about an 81% faradaic efficiency over a period of 18 min of electrolysis at a current density of about 236 mA cm^{-2} in 1 M KOH (Fig. S13), indicating the existence of efficient electron transfer during hydrogen production.

7. Conclusion

In conclusion, we have successfully synthesized vanadium doped nickel cobalt phosphide catalyst supported on carbon cloth by a facile hydrothermal and phosphorization method. On account of the strategy of heteroatom, acupuncture-shaped structure and the synergistic of transition bimetallic phosphide, more active sites are exposed and the electron transport rate is accelerated. The as-obtained V-NiCoP/CC exhibits an excellent HER activity with ultra-low η_{10} of 52 mV and a low tafel slope of 51.2 mV dec^{-1} in 1 M KOH solution. In terms of durability, V-NiCoP/CC shows a good stability after 2000 CV cycles and 40 h of long-term stability test, which will provide a feasible alternative to the noble metal catalyst solution. Furthermore, this work will broaden our horizons that we use a heteroatom doping technique to achieve electrochemical performance improvements in transition bimetallic or polymetallic phosphide catalysts.

CRediT authorship contribution statement

Xiao Li: Conceptualization, Methodology, Writing – original draft. **Yuanjian Liu:** Formal analysis. **Yudong Wu:** Data curation. **Shanshan Li:** Project administration. **Yinchen Dai:** Investigation. **Jibiao Guan:** Writing – review & editing. **Ming Zhang:** Supervision.

Declaration of Competing Interest

The authors declare that they have no known competing financial interests or personal relationships that could have appeared to influence the work reported in this paper.

Appendix A. Supplementary data

Supplementary data to this article can be found online at https://doi.org/10.1016/j.jelechem.2021.115812.

References

[1] R. Balderas-Xicohténcatl, P. Schmieder, D. Denysenko, D. Volkmer, M. Hirscher, High Volumetric Hydrogen Storage Capacity using Interpenetrated Metal-Organic Frameworks, Energy Technology 6 (3) (2018) 510–512.

[2] J. Liu, D. Zhu, Y. Zheng, A. Vasileff, S.-Z. Qiao, Self-Supported Earth-Abundant Nanoarrays as Efficient and Robust Electrocatalysts for Energy-Related Reactions, ACS Catal. 8 (7) (2018) 6707–6732.

[3] M. Ren, X. Lu, Y. Chai, X. Zhou, J. Ren, Q. Zheng, D. Lin, A three-dimensional conductive cross-linked all-carbon network hybrid as a sulfur host for high performance lithium-sulfur batteries, J Colloid Interface Sci 552 (2019) 91–100.

[4] A. Badruzzaman, A. Yuda, A. Ashok, A. Kumar, Recent advances in cobalt based heterogeneous catalysts for oxygen evolution reaction, Inorg. Chim. Acta 511 (2020).

[5] D. Wang, Q. Li, C. Han, Z. Xing, X. Yang, Single-atom ruthenium based catalyst for enhanced hydrogen evolution, Appl. Catal. B 249 (2019) 91–97.

[6] B. You, N. Jiang, M. Sheng, M.W. Bhushan, Y. Sun, Hierarchically Porous Urchin-Like Ni2P Superstructures Supported on Nickel Foam as Efficient Bifunctional Electrocatalysts for Overall Water Splitting, ACS Catal. 6 (2) (2015) 714–721.

[7] D.-J. Li, Q.-H. Li, Z.-G. Gu, J. Zhang, A surface-mounted MOF thin film with oriented nanosheet arrays for enhancing the oxygen evolution reaction, J. Mater. Chem. A 7 (31) (2019) 18519–18528.

[8] L. Zhao, Z. Yang, Q. Cao, L. Yang, X. Zhang, J. Jia, Y. Sang, H.-J. Wu, W. Zhou, H. Liu, An earth-abundant and multifunctional Ni nanosheets array as electrocatalysts and heat absorption layer integrated thermoelectric device for overall water splitting, Nano Energy 56 (2019) 563–570.

[9] Z. Ge, B. Fu, J. Zhao, X. Li, B. Ma, Y. Chen, A review of the electrocatalysts on hydrogen evolution reaction with an emphasis on Fe, Co and Ni-based phosphides, Journal of Materials Science 55 (29) (2020) 14081–14104.

[10] P. Zhou, D. Xing, Y. Liu, Z. Wang, P. Wang, Z. Zheng, X. Qin, X. Zhang, Y. Dai, B. Huang, Accelerated electrocatalytic hydrogen evolution on non-noble metal containing trinickel nitride by introduction of vanadium nitride, J. Mater. Chem. A 7 (10) (2019) 5513–5521.

[11] Y. Lin, Z. Yang, D. Cao, Y. Gong, Electro-deposition of nickel–iron nanoparticles on flower-like MnCo2O4 nanowires as an efficient bifunctional electrocatalyst for overall water splitting, CrystEngComm 22 (8) (2020) 1425–1435.

[12] Y. Li, M. Cui, T. Li, Y. Shen, Z. Si, H.-G. Wang, Embedding Co2P nanoparticles into co-doped carbon hollow polyhedron as a bifunctional electrocatalyst for efficient overall water splitting, Int. J. Hydrogen Energy 45 (33) (2020) 16540–16549.

[13] N. Cheng, S. Stambula, D. Wang, M.N. Banis, J. Liu, A. Riese, B. Xiao, R. Li, T.K. Sham, L.M. Liu, G.A. Botton, X. Sun, Platinum single-atom and cluster catalysis of the hydrogen evolution reaction, Nat Commun 7 (2016) 13638.

[14] B. Ma, Z. Yang, Z. Yuan, Y. Chen, Effective surface roughening of three-dimensional copper foam via sulfurization treatment as a bifunctional electrocatalyst for water splitting, Int. J. Hydrogen Energy 44 (3) (2019) 1620–1626.

[15] Y. Chen, R. Ren, Z. Wen, S. Ci, J. Chang, S. Mao, J. Chen, Superior electrocatalysis for hydrogen evolution with crumpled graphene/tungsten disulfide/tungsten trioxide ternary nanohybrids, Nano Energy 47 (2018) 66–73.

[16] X. Zhou, X. Yang, H. Li, M.N. Hedhili, K.-W. Huang, L.-J. Li, W. Zhang, Symmetric synergy of hybrid CoS2–WS2 electrocatalysts for the hydrogen evolution reaction, J. Mater. Chem. A 5 (30) (2017) 15552–15558.

[17] C. Tang, N. Cheng, Z. Pu, W. Xing, X. Sun, NiSe Nanowire Film Supported on Nickel Foam: An Efficient and Stable 3D Bifunctional Electrode for Full Water Splitting, Angew Chem Int Ed Engl 54 (32) (2015) 9351–9355.

[18] C. Du, M. Shang, J. Mao, W. Song, Hierarchical MoP/Ni2P heterostructures on nickel foam for efficient water splitting, J. Mater. Chem. A 5 (30) (2017) 15940–15949.

[19] N. Han, K.R. Yang, Z. Lu, Y. Li, W. Xu, T. Gao, Z. Cai, Y. Zhang, V.S. Batista, W. Liu, X. Sun, Nitrogen-doped tungsten carbide nanoarray as an efficient bifunctional electrocatalyst for water splitting in acid, Nat Commun 9 (1) (2018) 924.

[20] Q. Wang, H. Zhao, F. Li, W. She, X. Wang, L. Xu, H. Jiao, Mo-doped Ni2P hollow nanostructures: highly efficient and durable bifunctional electrocatalysts for alkaline water splitting, J. Mater. Chem. A 7 (13) (2019) 7636–7643.

[21] Y. Lu, W. Hou, D. Yang, Y. Chen, CoP nanosheets in-situ grown on N-doped graphene as an efficient and stable bifunctional electrocatalyst for hydrogen and oxygen evolution reactions, Electrochim. Acta 307 (2019) 543–552.

[22] Y. Zhou, Y. Yang, R. Wang, X. Wang, X. Zhang, L. Qiang, W. Wang, Q. Wang, Z. Hu, Rhombic porous CoP2 nanowire arrays synthesized by alkaline etching as highly active hydrogen-evolution-reaction electrocatalysts, J. Mater. Chem. A 6 (39) (2018) 19038–19046.

[23] Y. Lei, M. Jia, P. Guo, J. Liu, J. Zhai, MoP nanoparticles encapsulated in P-doped carbon as an efficient electrocatalyst for the hydrogen evolution reaction, Catal. Commun. 140 (2020).

[24] J. Zhang, X. Cao, M. Guo, H. Wang, M. Saunders, Y. Xiang, S.P. Jiang, S. Lu, Unique Ni Crystalline Core/Ni Phosphide Amorphous Shell Heterostructured Electrocatalyst for Hydrazine Oxidation Reaction of Fuel Cells, ACS Appl Mater Interfaces 11 (21) (2019) 19048–19055.

[25] H. Xiong, G. Sun, Z. Liu, L. Zhang, L. Li, W. Zhang, F. Du, Z.A. Qiao, Polymer Stabilized Droplet Templating towards Tunable Hierarchical Porosity in Single Crystalline Na3 V2 (PO4)3 for Enhanced Sodium-Ion Storage, Angew Chem Int Ed Engl 60 (18) (2021) 10334–10341.

[26] S. Li, Y. Wu, X. Du, Y. Fang, L. Wang, J. Yao, I. Krucinska, M. Zhang, Self-supported Mo0.2Co0.8P nanowire arrays on carbon cloth as a high-performance and durable hydrogen evolution reaction electrocatalyst in wide-range pH, Journal of Electroanalytical Chemistry 888 (2021).

[27] Y. Zheng, R. Zhang, L. Zhang, Q. Gu, Z.A. Qiao, A Resol-Assisted Cationic Coordinative Co-assembly Approach to Mesoporous ABO3 Perovskite Oxides with Rich Oxygen Vacancy for Enhanced Hydrogenation of Furfural to Furfuryl Alcohol, Angew Chem Int Ed Engl 60 (9) (2021) 4774–4781.

[28] H. Xiong, H. Zhou, G. Sun, Z. Liu, L. Zhang, L. Zhang, F. Du, Z.A. Qiao, S. Dai, Solvent-Free Self-Assembly for Scalable Preparation of Highly Crystalline Mesoporous Metal Oxides, Angew. Chem. Int. Ed. 59 (27) (2020) 11053–11060.

[29] C. Ray, S.C. Lee, B. Jin, A. Kundu, J.H. Park, S.C. Jun, Stacked Porous Iron-Doped Nickel Cobalt Phosphide Nanoparticle: An Efficient and Stable Water Splitting Electrocatalyst, ACS Sustainable Chem. Eng. 6 (5) (2018) 6146–6156.

[30] Z. Zhou, N. Mahmood, Y. Zhang, L. Pan, L. Wang, X. Zhang, J.-J. Zou, CoP nanoparticles embedded in P and N co-doped carbon as efficient bifunctional electrocatalyst for water splitting, Journal of Energy Chemistry 26 (6) (2017) 1223–1230.
[31] T. Wang, Y. Sun, L. Zhang, K. Li, Y. Yi, S. Song, M. Li, Z.A. Qiao, S. Dai, Space-Confined Polymerization: Controlled Fabrication of Nitrogen-Doped Polymer and Carbon Microspheres with Refined Hierarchical Architectures, Adv Mater 31 (16) (2019) e1807876.
[32] W. Hua, H. Sun, L. Ren, D. Nan, V-Doped CoP Nanosheet Arrays as Highly Efficient Electrocatalysts for Hydrogen Evolution Reaction in Both Acidic and Alkaline Solutions, Front Chem 8 (2020) 608133.
[33] K.N. Dinh, P. Zheng, Z. Dai, Y. Zhang, R. Dangol, Y. Zheng, B. Li, Y. Zong, Q. Yan, Ultrathin Porous NiFeV Ternary Layer Hydroxide Nanosheets as a Highly Efficient Bifunctional Electrocatalyst for Overall Water Splitting, Small 14 (8) (2018).
[34] X. Wang, Y. Chen, J. He, B. Yu, B. Wang, X. Zhang, W. Li, M. Ramadoss, W. Zhang, D. Yang, Vertical V-Doped CoP Nanowall Arrays as a Highly Efficient and Stable Electrocatalyst for the Hydrogen Evolution Reaction at all pH Values, ACS Applied Energy Materials 3 (1) (2019) 1027–1035.
[35] D. Chen, R. Lu, Z. Pu, J. Zhu, H.-W. Li, F. Liu, S. Hu, X. Luo, J. Wu, Y. Zhao, S. Mu, Ru-doped 3D flower-like bimetallic phosphide with a climbing effect on overall water splitting, Appl. Catal. B 279 (2020).
[36] X. Tong, N. Pang, Y. Qu, C. Yan, D. Xiong, S. Xu, L. Wang, P.K. Chu, 3D urchin-like NiCo2O4 coated with carbon nanospheres prepared on flexible graphite felt for efficient bifunctional electrocatalytic water splitting, J. Mater. Sci. 56 (16) (2021) 9961–9973.
[37] M. Yang, X. Fu, M. Shao, Z. Wang, L. Cao, S. Gu, M. Li, H. Cheng, Y. Li, H. Pan, Z. Lu, Cobalt-Vanadium Hydroxide Nanoneedles with a Free-Standing Structure as High-Performance Oxygen Evolution Reaction Electrocatalysts, ChemElectroChem 6 (7) (2019) 2050–2055.
[38] J.-F. Qin, J.-H. Lin, T.-S. Chen, D.-P. Liu, J.-Y. Xie, B.-Y. Guo, L. Wang, Y.-M. Chai, B. Dong, Facile synthesis of V-doped CoP nanoparticles as bifunctional electrocatalyst for efficient water splitting, Journal of Energy, Chemistry 39 (2019) 182–187.
[39] J. Wang, W. Yang, J. Liu, CoP2nanoparticles on reduced graphene oxide sheets as a super-efficient bifunctional electrocatalyst for full water splitting, J. Mater. Chem. A 4 (13) (2016) 4686–4690.
[40] A. Sivanantham, P. Ganesan, S. Shanmugam, Hierarchical NiCo2S4Nanowire Arrays Supported on Ni Foam: An Efficient and Durable Bifunctional Electrocatalyst for Oxygen and Hydrogen Evolution Reactions, Adv. Funct. Mater. 26 (26) (2016) 4661–4672.
[41] Z. Liu, J. Wang, C. Zhan, J. Yu, Y. Cao, J. Tu, C. Shi, Phosphide-oxide honeycomb-like heterostructure CoP@CoMoO4/CC for enhanced hydrogen evolution reaction in alkaline solution, J. Mater. Sci. Technol. 46 (2020) 177–184.
[42] M. Hao, M. Xiao, L. Qian, Y. Miao, Synthesis of cobalt vanadium nanomaterials for efficient electrocatalysis of oxygen evolution, Front. Chem. Sci. Eng. 12 (3) (2018) 409–416.
[43] J. Liu, J. Cui, J. Sun, H. Liu, W. Li, C. Han, Y. Chen, G. Yang, Y. Shan, Hierarchical nickel-vanadium nanohybrid with strong electron transfer for accelerated hydrogen evolution reaction, Appl. Surf. Sci. 528 (2020).
[44] Q. Zhu, M. Shao, S.H. Yu, X. Wang, Z. Tang, B. Chen, H. Cheng, Z. Lu, D. Chua, H. Pan, One-Pot Synthesis of Co-Doped VSe2 Nanosheets for Enhanced Hydrogen Evolution Reaction, ACS Applied Energy Materials 2 (1) (2018) 644–653.
[45] K. Fan, Y. Ji, H. Zou, J. Zhang, B. Zhu, H. Chen, Q. Daniel, Y. Luo, J. Yu, L. Sun, Hollow Iron-Vanadium Composite Spheres: A Highly Efficient Iron-Based Water Oxidation Electrocatalyst without the Need for Nickel or Cobalt, Angew Chem Int Ed Engl 56 (12) (2017) 3289–3293.
[46] L. Wen, J. Yu, C. Xing, D. Liu, X. Lyu, W. Cai, X. Li, Flexible vanadium-doped Ni2P nanosheet arrays grown on carbon cloth for an efficient hydrogen evolution reaction, Nanoscale 11 (10) (2019) 4198–4203.
[47] R. Zhang, C. Tang, R. Kong, G. Du, A.M. Asiri, L. Chen, X. Sun, Al-Doped CoP nanoarray: a durable water-splitting electrocatalyst with superhigh activity, Nanoscale 9 (14) (2017) 4793–4800.
[48] Y. Zhang, K. Xu, B. Zhang, S. Guan, X. Fu, Z. Peng, Pr-doped NiCoP nanowire arrays for efficient hydrogen evolution in both acidic and alkaline media, J. Alloy. Compd. 862 (2021).
[49] Y. Pan, Y. Liu, J. Zhao, K. Yang, J. Liang, D. Liu, W. Hu, D. Liu, Y. Liu, C. Liu, Monodispersed nickel phosphide nanocrystals with different phases: synthesis, characterization and electrocatalytic properties for hydrogen evolution, J. Mater. Chem. A 3 (4) (2015) 1656–1665.
[50] C.C.L. McCrory, S. Jung, J.C. Peters, T.F. Jaramillo, Benchmarking Heterogeneous Electrocatalysts for the Oxygen Evolution Reaction, J. Am. Chem. Soc. 135 (45) (2013) 16977–16987.
[51] X. Du, Y. Fang, J. Guan, S. Li, L. Wang, M. Zhang, Vanadium doped cobalt phosphide nanorods array as a bifunctional electrode catalyst for efficient and stable overall water splitting, Int. J. Hydrogen Energy 46 (1) (2021) 599–608.
[52] Q. Qian, J. Zhang, J. Li, Y. Li, X. Jin, Y. Zhu, Y. Liu, Z. Li, A. El-Harairy, C. Xiao, G. Zhang, Y. Xie, Artificial Heterointerfaces Achieve Delicate Reaction Kinetics towards Hydrogen Evolution and Hydrazine Oxidation Catalysis, Angew Chem Int Ed Engl 60 (11) (2021) 5984–5993.
[53] X. Lu, W.L. Yim, B.H. Suryanto, C. Zhao, Electrocatalytic oxygen evolution at surface-oxidized multiwall carbon nanotubes, J Am Chem Soc 137 (8) (2015) 2901–2907.
[54] A.P. Grosvenor, S.D. Wik, R.G. Cavell, A. Mar, Examination of the Bonding in Binary Transition-Metal Monophosphides MP (M: Cr, Mn, Fe, Co) by X-Ray Photoelectron Spectroscopy, ChemInform 37 (6) (2006).